Diagnostic study of geomagnetic storm-induced ionospheric changes over VLF signal propagation paths in mid-latitude D-region

Victor U. J. Nwankwo[1], Sandip K. Chakrabarti[2], William Denig[3], Olugbenga Ogunmudimu[4], Muyiwa P. Ajakaiye[1], and Paul Anekwe[1]

[1]Space, Atmospheric and Radiowave Propagation Laboratory, Department of Physics, Anchor University, Lagos, Nigeria
[2]Indian Centre for Space Physics, Kolkata-700084, India
[3]St. Joseph College of Maine, Standish, ME 04084, U.S.A
[4]Department of Electrical Engineering, Manchester Metropolitan University, Manchester, UK

Correspondence: Victor U. J. Nwankwo (vnwankwo@aul.edu.ng)

Abstract. We performed a diagnostic study of geomagnetic storm-induced disturbances that are coupled to the lower ionosphere in mid-latitude D-region using propagation characteristics of VLF radio signals. We characterised the diurnal VLF amplitude (from two propagation paths) into five metrics, namely the mean amplitude before sunrise (MBSR), midday amplitude peak (MDP), mean amplitude after sunset (MASS), sunrise terminator (SRT) and sunset terminator (SST). We analysed
5 and monitored the trend in variations of signal metrics for up to 20 storms, to understand deviations in the signal that are attributable to the storms; five storms (and their effects on the signals) were studied in detail, followed by statistical analysis that included 15 other events. When the pre-storm day signal level where compared with the storm day values, we found that the MDP exhibited characteristic dipping in about 67% and 80% in GQD-A118 and DHO-A118 propagation paths, respectively. The MBSR showed respective dipping of about 77% and 60%, while the MASS dipped by 58% and 67%. Conversely, the
10 SRT and SST showed respective dipping of 25% and 33%, and 42% and 47%. The percentage dip of the MBSR and MASS increased significantly when the 2-day mean signals before the events (as against the 1-day mean value) were cosidered. Of the two propagation paths used in this study, the dipping of the amplitude of DHO-A118 propagation path signal is larger (as also observed in previous study). To understand the state of the ionosphere over the signal propagation paths and how it affects the VLF responses, we further analysed virtual heights (h'E, h'F1 and h'F2) and critical frequencies (f_oE, f_oF1, and f_oF2) of
15 the E and F regions (from ionosonde stations near the transmitters). The results of this analysis showed a significant increase and/or fluctuations of the foF2, foF1, h'F2, h'F, h'Es and h'E near both transmitters during the geomagnetic storms. The largest increase in heights of the regions (h'F2, h'F, h'Es and h'E) occured over Juluisruh station (around the DHO transmitter) in Germany, suggesting a strong storm responses over the region leading to the large dipping of the DHO-A118 propagation path signal.

1 Introduction

The size, shape and behaviour of the magnetosphere (formed by the interaction between the solar wind and the Earth's magnetic field) are controlled by the varying properties of the solar wind plasma and the embedded magnetic fields (McPherron et al., 2008). Solar-induced geomagnetic footprints in the magnetosphere are coupled to the ionosphere through the linkage of the Earth's magnetic field despite their large distance apart, thus making the regions physically connected into a single global system (Nwankwo et al., 2016). Geomagnetic storms (and associated substorms) are the leading driver of large-scale coupled magnetosphere-ionosphere perturbations in the geospace, and are mainly product of strong variations in solar wind conditions via energy transfer. Sustained periods of high speed solar wind (HSS), and a southward directed solar wind magnetic field at the dayside of the magnetosphere largely favours the initiation of geomagnetic storms (Lastovicka, 1989, 1996; Tsurutani et al., 1995, 2006, 2011; Baker D. N., 2000; Borovsky and Denton, 2006; Kozyra, 2006; McPherron et al., 2008). The momentary eruption of large-scale, high-mass plasma (in solar wind) known as coronal mass ejections (CMEs), and the corotating interactive regions (CIRs) formed when HSS interacts with preceding low-speed solar winds, can interact with the magnetosphere, potentially initiating geomagnetic disturbances and/or storm condition (Gosling and Pizzo, 1999; Borovsky and Denton, 2006; Tsurutani et al., 2011). CME-induced geomagnetic storms are often large, more geo-effective and frequent during solar maxima, while HSS/CIR-induced storms are usually less intense and dominates the declining phase of the solar cycle. However, more energy is transferred (or, deposited) to the magnetosphere during HSS/CIR induced storms, which last for longer duration (a week or more) than the CME-induced storm scenario (Tsurutani et al., 2011; Verkhoglyadova et al., 2013). The perturbations produced by storms in the magnetosphere are coupled to the ionosphere where they produce a large variety of space weather disturbances.

In the ionosphere, effects of geomagnetic storms manifest mainly through joule heating, and precipitation of energetic particles especially below the dynamo region, ~95-100 km (Lastovicka, 1996), causing significant enhancement of electron density (Chenette et al., 1993; Stoker P. H., 1993; Lastovicka, 1996), and modulation of galactic cosmic ray flux, global electric circuit, and atmospheric electricity (Danilov and Lastovicka, 2001). The ionosphere also responds to prompt changes due to solar flares associated bursts in EUV, X-ray and relativistic particles (Mitra, 1974; Buonsanto, 1999; Alfonsi et al., 2008). These manifestations can modify atmospheric parameters (Nwankwo et al., 2016), leading to irregularities that can affect the operational capabilities of space-based systems and alteration of the reflection conditions for radio waves propagating in the Earth-ionosphere waveguide (EIWG). Substantial progress has been made in understanding global dynamics and large-scale coupling of the upper ionosphere using both ground-based observational capabilities (e.g., Global Navigation Satellite System (GNSS) receivers, vertical and oblique high frequency (HF) sounding, atmospheric radar (coherent and incoherent scatter radars)) and space-based satellite systems (e.g., Advance Composition Explorer (ACE), Constellation Observing System for Meteorology, Ionosphere and Climate (COSMIC), Defense Meteorological Satellite Program (DMSP), Geostationary Operational Environmental Satellite (GOES) etc.) (Nwankwo et al., 2020d). However, the physics of lower ionospheric coupling in terms of solar wind driving remains a major scientific gap because of the limited observational capabilities in the lower

55 ionosphere, especially satellite systems. Putting satellites in orbits lower than 200 km is both challenging and expensive.

VLF radiowaves is one of the tool deployed for monitoring and studying changes in the lower atmosphere/ionosphere (up to 95 km), because their amplitude and phase are sensitive to changes in electrical conductivity of the ionosphere (Alfonsi et al., 2008). The study of trends in variation of diurnal VLF narrowband is proving to be useful to understand space weather
60 effects in the lower ionosphere (e.g. Araki T. (1974); Kikuchi and Evans (1983); Kleimenov et al. (2004); Peter et al. (2006); Cliverd et al. (2010); Kumar and Kumar (2014); Tatsuta et al. (2015); Nwankwo et al. (2016)), as well as ionospheric changes from other atmospheric and lithospheric sources. Solar flare/X-ray flux-induced ionospheric disturbances in the D-region are normally detected as a sudden change in VLF amplitude and phase. The VLF detection mechanism of flare-induced sudden ionospheric disturbances (SID) in D region are described in Nwankwo et al. (2016). The signal can also be significantly affected
65 by geomagnetic disturbances and/or storm-induced ionosphere perturbations (Kikuchi and Evans, 1983). While the daytime signal amplitude and phase are well correlated with X-ray flux induced SID and well studied, geomagnetic storm-induced disturbances appear not to be visibly detectable on the signal's signature. However, their responses to geomagnetic storms has been shown to manifest through amplitude (and/or phase) depression (or dipping) and fluctuation. Kikuchi and Evans (1983) reported the occurrence of VLF phase anomaly associated with sub-storm of 13 November 1979 in trans-auroral propagation
70 path. Peter et al. (2006) reported the depression of VLF signal amplitude of up to 5 dB in magnitude in mid-latitude during storms of 7 April 2000 and 31 October 2003, and later observed in lower latitudes. Kumar and Kumar (2014) later reported a depression in VLF signal strength in low latitude during severe storm condition of 15 December 2006. Nwankwo et al. (2016) also reported significant dipping of VLF mid-day signal amplitude (MDP), mean signal amplitude before sunrise (MBSR) and mean signal amplitude before sunset (MASS) in majority of 16 storm cases studied in mid-latitude during February 2011 to
75 June 2012.

Although there are similarities in the work of these authors (shedding light on VLF response to storms), Nwankwo et al. (2016) have, in addition, characterised the amplitude of the diurnal VLF amplitude variation into distinct metrics (e.g., MBSR, MDP, MASS, SRT and SST) and included several cases of storms with the aim of bringing statistical significance into the
80 analysis. They also observed some incidences of MDP signal rise (or, increase) during some storms despite significant dipping in majority of the signal. Nwankwo et al. (2020d) noted that some signal propagation paths may not exhibit the storm-induced dipping and/or may do so for some storms due to factors such as mode interference, propagation path and anti-correlated responses of VLF signal to a combination of storm induced and/or enhanced ionospheric phenomena (e.g., prompt penetration electric fields (PPEFs) and disturbance dynamo electric field (DDEF)), and strong solar flares occuring simultaneously. How-
85 ever, to understand their propagation characteristics it is important to monitor the state of the ionosphere over the propagation paths of VLF radio waves when probing ionospheric irregularities using the signal (Nwankwo et al., 2020d). This will require simultaneous combination of observed VLF amplitude/phase variations in the lower ionosphere with parameter that defines the state of the ionospheric (e.g., total electron content (TEC), ionosode etc.) over the signal propagation paths.

There is a unique relationship exist between the sounding frequency of high-frequency (HF) radio pulses and ionospheric ionisation densities (especially in the E and F region) that can reflect it. Values of the virtual heights of E and F layers (denoted by h'E, h'F1 and h'F2), and their critical frequencies (denoted by foE, foF1, and foF2) are scaled from ionograms produced by an ionosonde (National Geographic Data Centre, 1996). Similarly, the electron density (N_mF2) of F2 ionospheric region can also be measured (e.g., (Sica and Schunk, 1990; Buresova and Lastovicka, 2007; Chuo et al., 2013)). These parameters can be used to monitor the state of the ionosphere in the E and F regions. The F region is the most sensitive area of the ionosphere, and reflects important dynamics of the ionosphere. Hence, majority of ionospheric studies are related to the region (Chuo et al., 2013). In previous studies, measured N_mF2 have been used to estimate the height of the F2 peak, h_mF2 (Sica and Schunk, 1990), and strong pre-storm enhancements of the parameter (N_mF2) have been reported in high- to mid-latitudes (Buresova and Lastovicka, 2007). It has also been shown that nearly all ionospheric parameters (e.g. foF2, foF1, foE, foEs, h'F2, h'E, h'Es) exhibit 11-year solar cycle evolution (Ouattara et al., 2009). This characteristic demonstrates their sensitivity to solar activity (Nwankwo et al., 2020d), and therefore, a strong indication that space weather effects on the ionosphere can be monitored using these parameters. In this work, we combine the observed diurnal VLF amplitude variation in the D-region with HF radio pulses in the E and F regions (ionosonde) to perform a diagnostic investigation of coupled geomagnetic storm effects, in order to understand the observed storm-induced variations in VLF narrowband based on the state and responses of ionosphere. Similar analysis (or study) has also been done using TEC/VTEC indices (Nwankwo et al., 2020d).

2 Data and Method

We obtained the VLF amplitude (diurnal) data for DHO-A118 and GQD-A118 propagation paths received at A118 SID monitoring station in Southern France (Muret). The location of the transmitters (GQD (22.1 kHz GQD, lat N54.73° long W002.88°) and DHO (23.4 kHz, lat N53.08° long W007.61°)) and the receiver (A118) are depicted in Figure 1. The the DHO and GQD transmitters and the A118 receiver are 1169.18 km and 1315.66 km, respectively. Other data include GOES solar X-ray flux, solar wind speed (V_{sw}) and particle density (PD) (ftp://sohoftp.nascom.nasa.gov/sdb/goes/ace/), planetary geomagnetic A_p (from NOAA) and the disturbance storm time (Dst) index (from World Data Centre for Geomagnetism (WDCG)). These data were described in detail in Nwankwo et al. (2016) and references therein.

The analysed intervals are 16th-31st September and 22 October-5 November 2011. The geomagnetic storms of interest within the intervals include the events on 17, 26-27 September, 25 October and 1 November 2011. We monitor variation 2-4 hour mean VLF signal amplitude before local sunrise and after sunset (hereafter respectively denoted as MBSR and MASS), and the mid-day signal amplitude peak (MDP). We note that the acronym DTMA (daytime mean amplitude) was used in Nwankwo et al. (2020d) instead of the MDP. The difference between the two metrics is that DTMA represent 1-hour mean value of daytime amplitude, while MDP is a single value of the signal amplitude around midday. We also identified typical values of the signal at sunrise and sunset, also recognised as sunrise and sunset terminators (hereafter, denoted as SRT and SST). The diurnal VLF amplitude indicating portion of the characterised metrics (MBSR, MDP, MASS, SRT and SST) are shown in Fig.

Figure 1. VLF signal propagation paths (DHO-A118 and GQD-A118) used in the study

2a. The signals were analysed in conjunction with geomagnetic indices, to describe storm-induced magnetosphere-ionosphere coupling in mid-latitude D region. We thus study the trend in variations of these key metrics under varying geomagnetic storm
125 conditions using the signal propagation characteristics, to understand behaviours attributable to geomagnetic storm-induced variations in the lower ionosphere (besides the visible response of the signal's amplitude and/or phase associated with solar flare/X-ray flux).

3 Results and Discussion

3.1 Analysis of VLF amplitude variations during intervals of geomagnetic storms

130 Figure 3 shows the diurnal VLF amplitude for (a) DHO-A118 and (b) GQD-A118 propagation paths, daily variation in (c) X-ray flux output (d) solar wind speed (V_{sw}) (e) solar particle density (PD) (f) Disturbance storm time (Dst) (g) planetary geomagnetic A_p and (h) Auroral Electrojet (AE) indices during 16-30 September 2011. Four storm conditions were recorded during the period - moderate storm on 17th (Dst=-60) and consecutive storms on 26th (Dst=-101), 27th (Dst=-88) and 28th (Dst=-62), presumably driven by the significant increase in V_{sw} and PD on 17th and 26th (Fig. 3a-f). However, the main refer-
135 ence storms are those of 17th and 26th. The variation of the AE (especially between 26th and 29th) appear to be consistent with high-intensity, long-duration continuous AE activity events (HILDCAAs). Hence, 'fresh energy was injected' into the magnetosphere in the process (Tsurutani et al., 2011). We observed a notable drop in DHO-A118 VLF signal level on 26th around midday following the relatively intense storm condition with Dst up to -101 (Fig. 3a). This scenario (signal strength decrease) have been associated with storm-induced variations in energetic electron precipitation flux (Kikuchi and Evans, 1983; Peter et
140 al., 2006). During a geomagnetic storm, the current system in the ionosphere, and the energetic particles that precipitate into the ionosphere deposit energy in the form of heat that can influence the density and distribution of density in the atmosphere
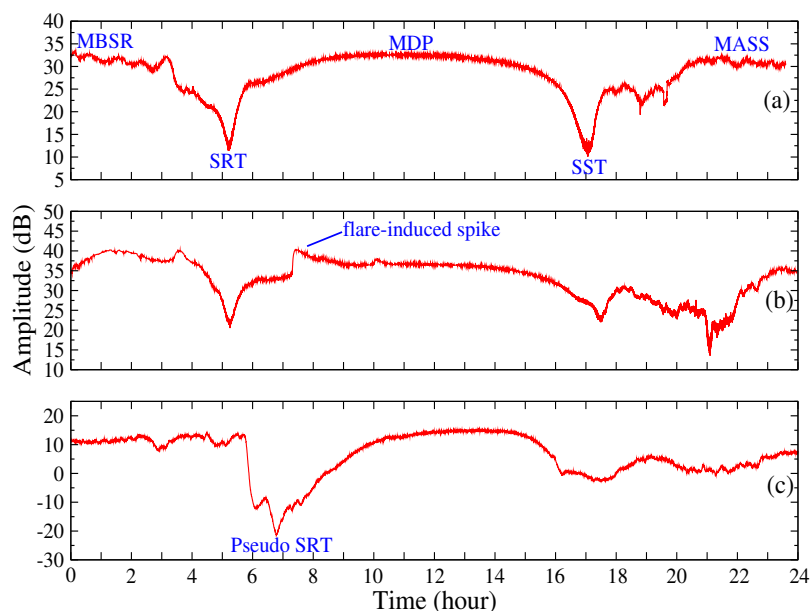
Figure 2. Diurnal VLF signal amplitude signatures showing analysed signal metrics

(NOAA4, 2016). The characterised metrics (e.g., MBSR, MDP, MASS, SST and SRT) of the VLF signal amplitude makes it easier to study the behaviour of the signal during the storms by monitoring their trends of variation. We therefore monitor trends of the signals variation for possible detection of storm induced signatures in the lower ionosphere where the signals are reflected and/or propagated.

Figure 4 shows daily mean fluctuation of Dst and AE, and variations in the VLF midday signal amplitude peak (MDP), mean signal amplitude before local sunrise (MBSR), mean signal amplitude after sunset (MASS), sunrise terminator (SRT) and sunset terminator (SST) for (a) DHO-A118 and (b) GQD-A118 propagation paths during 16-30 September 2011. In GQD-A118 propagation path (Fig. 4a), we observed a dipping of the MDP on 17th (extending to 20th), as well as dipping of the MASS on 17 Sept., but an increase of the MBSR, SRT and SST. Following the recurrent storms between 26 and 28 Sept., we observed dipping of the MDP on 26 Sept (extending to 29th). The slight increase of the signal (MDP) on 28th appear to be due to the significant flare activity (3 C-class and 1 M-class), suggesting increase in both the instantaneous and background X-ray flux output that usually results to spike in signal amplitude (depicted in figure 2b). High flare activity often overshadows the signal's response to geomagnetic storms when significant flare and storm events occur simultaneously (Nwankwo et al., 2016). There is also a significant dipping of all the signal metrics (MDP, MBSR, MASS, SRT and SST) on 27 Sept. We note dipping of the MBSR on the days following the main (reference) storms on 18 and 27 Sept. Since the events occurred after dawn (around midday), the post-storm ionospheric effects are expected well into the day following the storm. This trend (post-storm day signal dip), suggest that the signals dipped in response to continuous driving of the ionospheric on the days following the
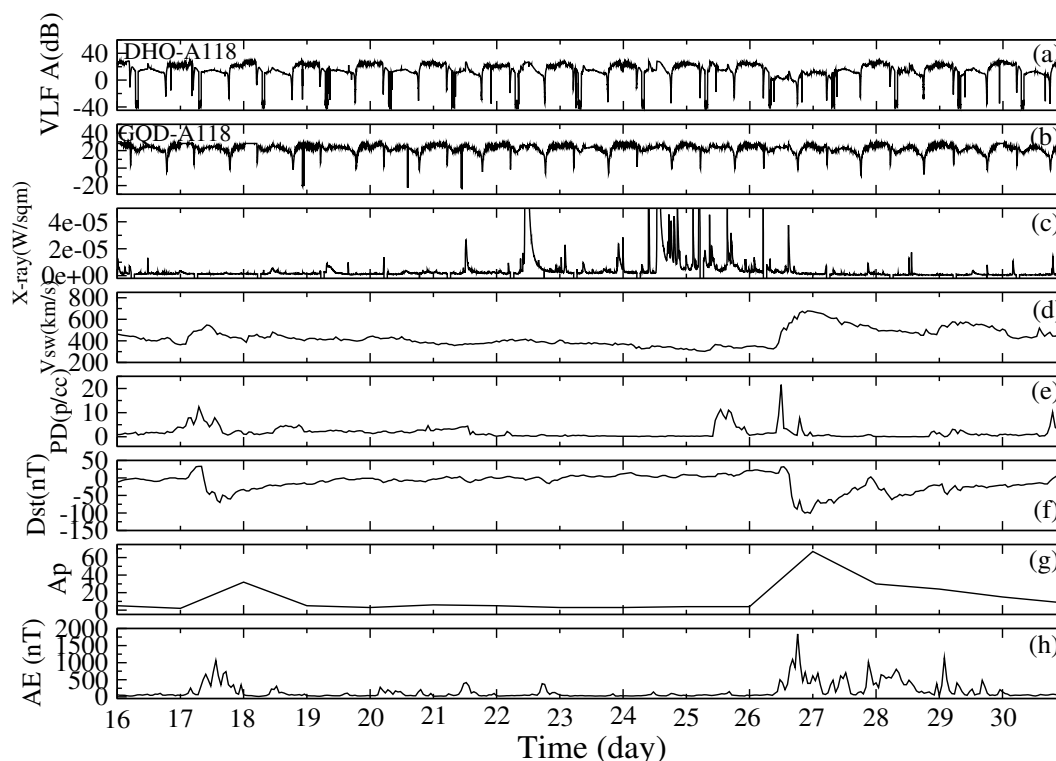
Figure 3. (a) Diurnal VLF amplitude for DHO-A118 and (b) GQD-A118 propagation paths (c) daily variation in X-ray flux output (d) solar wind speed (V_{sw}) (e) solar particle density (PD) (f) Disturbance storm time (Dst) (g) planetary A_p and (h) Auroral Electrojet (AE) indices during 16-30 September 2011

160   events. However, such response also depend on the characteristics of the signals propagation path. In DHO-A118 propagation path, dipping of the MDP, MBSR, SRT and SST occurred on 17 Sept., and only the MDP, MASS and SST decreased on 26 Sept. The MASS and SRT maintained the pre-storm day values of 16 and 25 Sept., respectively. While the MBSR increased slightly on 26th (main storm day), there is a significant dipping of the signal following recurrent storm of 27 Sept.

165   Figure 5 shows diurnal VLF amplitude for (a) DHO-A118 and (b) GQD-A118 propagation paths, daily variation in (c) X-ray flux output (d) V_{sw} (e) PD (f) Dst (g) A_p and (h) AE indices during 22 October - 5 November 2011. This period is associated with three storms - a severe storm with main phase on 25th October (Dst=-132) and consecutive storms on 1 November (Dst=-71) and 2nd November (Dst=-57), presumably induced by the highly variable V_{sw} and PD (Fig. 5d-e). It has been shown that the capability of a given value of the solar wind electric field (SWEF) to create a Dst disturbance or

170   geo-efficiency is enhanced by high solar wind density (Weigel, 2010; Tsurutani et al., 2011). Variation of the AE between 30 Oct. and 3rd Nov. also appear to be consistent with HILDCAAs (Fig. 5h). The DHO-A118 VLF signal level on 25 Oct. around midday also showed a visible reduction following the intense storm condition with Dst up to -132 (Fig. 5a). VLF signal data
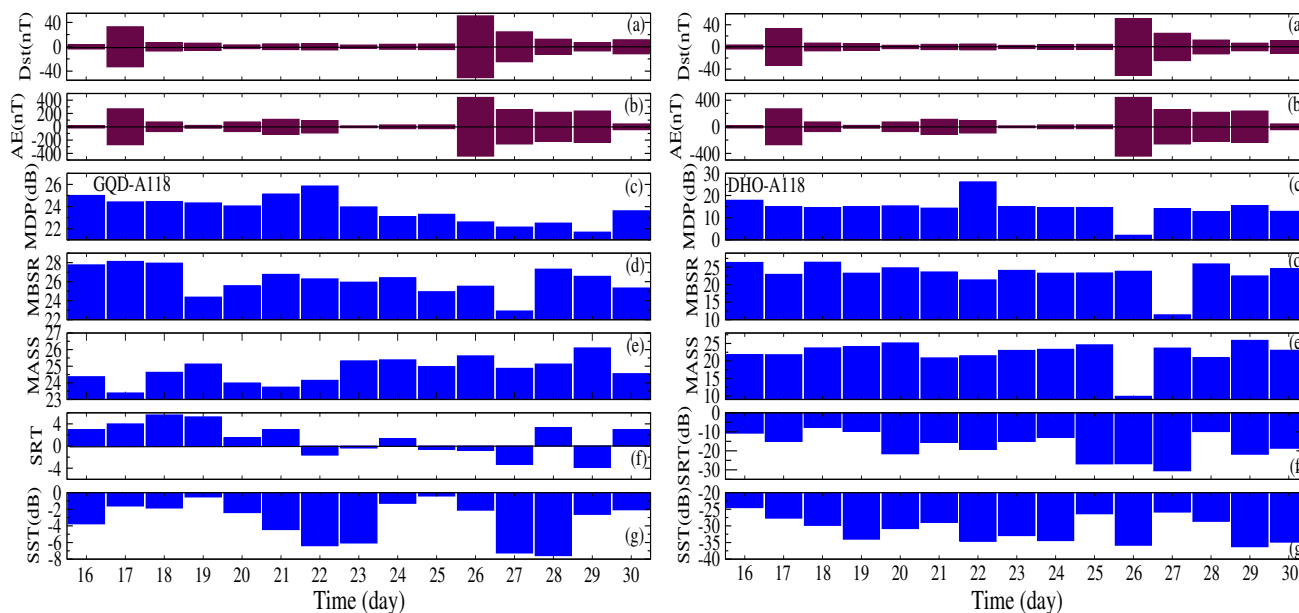
Figure 4. Daily deviations of (a) Dst (b) AE (c) variations in the peak value of midday signal amplitude (MDP) (d) mean signal amplitude before local sunrise (MBSR) (e) mean signal amplitude after sunset (MASS) (f) variation in sunrise terminator (SRT) and (g) sunset terminator (SST) for GQD-A118 (left panel) and DHO-A118 (right panel) propagation paths during 16-30 September 2011.

for GQD-A118 propagation path are not available during 12:00 noon, 25 Oct. to 06:00 pm on 26th October (Fig. 5b).

175   Figure 6 shows daily deviations of Dst and AE, and variations in the MDP, MBSR, MASS, SRT and SST for (a) DHO-A118 and (b) GQD-A118 propagation paths during 22 October - 5 November 2011. Although data for GQD-A118 propagation path during 25 and 26 October is inadequate for the present analysis, we did observe a dipping of the MBSR on the main storm day (25 Oct.). Dipping of the MDP, MASS and SST occurred on 1 Nov., and those of MBSR, MASS, and SRT on 2 Nov., following the consecutive storms. In DHO-A118 propagation path, we observed dipping of the MDP, MBSR, MASS, and SRT

180 on 25 Oct., dipping of the MDP, MBSR, MASS, and SST on 1st Nov., and dipping of the MBSR and SRT on 2 Nov. Similar to the first case (Figs. 4 and 5), we note the high flare events on 2nd Nov (up to 7 C-class and 1 M-class), that may have caused a spike in the MDP on the day in both GQD-A118 and DHO-A118 propagation paths. Although dipping of the MDP signal (following storm events) has shown a considerable consistency across the cases presented so far, the MBSR and MASS (in particular) appear to be influenced by storms occurrence time and the high variability or fluctuation of the dusk-to-dawn

185 ionosphere (and signal) (Nwankwo et al., 2016). However, presenting a consistency across a substantial number of cases is vital to the conclusion of this work. Against this backdrop, we statistically analyse 15 more storm cases between September 2011 and October 2012 in order to obtain the statistical significance of the observations. The 15 storm cases are presented in
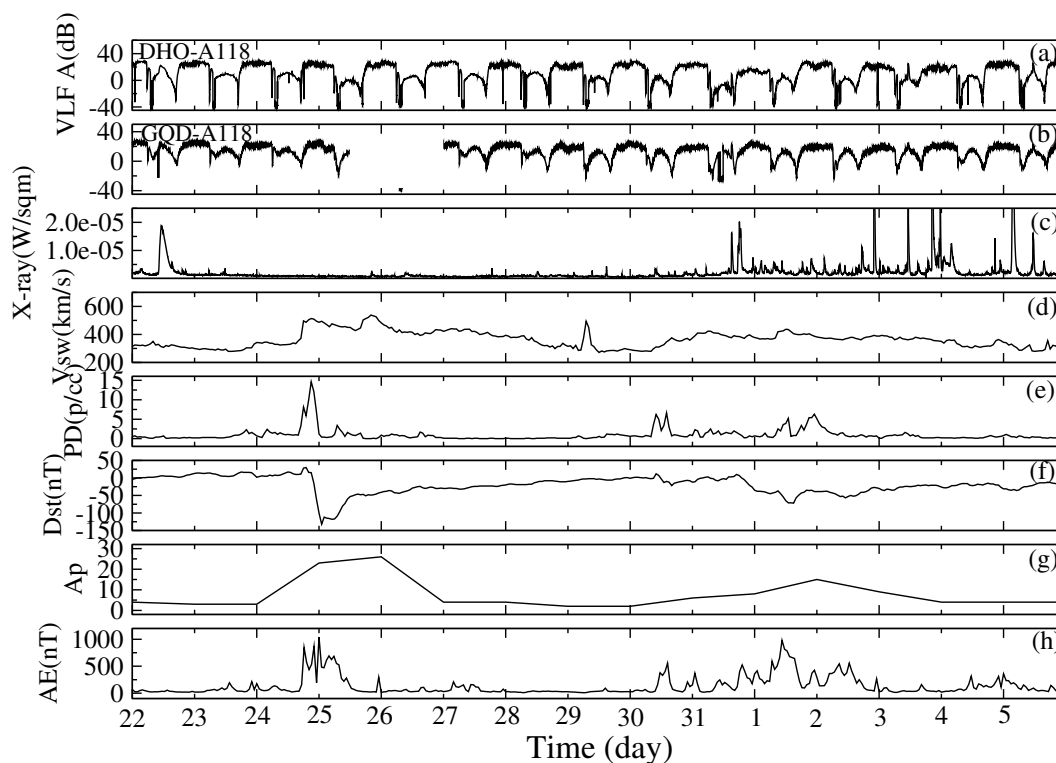
Figure 5. (a) Diurnal VLF amplitude for DHO-A118 and (b) GQD-A118 propagation paths (c) daily variation in X-ray flux output (d) solar wind speed (V_{sw}) (e) solar particle density (PD) (f) Disturbance storm time (Dst) (g) planetary A_p and (h) Auroral Electrojet (AE) indices during 22 October to 5 November 2011

Table 1, which excluded some cases that were previously analysed in Nwankwo et al. (2016) but included new cases.

190   In Figure 7, we show Dst deviation or fluctuation and trend in variation of the MDP, MBSR, MASS, SRT and SST signals during successive one-day before and after each of the 15 selected storm cases for (a) GQD-A118 and (b) DHO-A118 propagation paths. We recognised 3 consecutive days - as day before an even (BE), during event (DE) and after event (AEv). A '0' indicate absence of data. It should be noted however (for this analysis) that these events are separate events, and not continuous events. In GQD-A118 propagation path, about 8 of 12 MDP, 10 of 13 MBSR, 7 of 12 MASS, 3 of 12 SRT and

195   5 of 12 SST showed dipping, while 12 of 15 MDP, 9 of 15 MBSR, 10 of 15 MASS, 5 of 15 SRT and 7 of 15 SST showed dipping in DHO-A118 propagation path. These values correspond to 73.5%, 68.5%, 62.5%, 29.0% and 44.5% of the combined cases, respectively. The signal levels, along with the percentage dip are presented in Table 2. The MDP signals (in both the propagation paths) have generally shown remarkable evidence of dipping following geomagnetic storm conditions. However, we did also observe few scenarios of increase (of MDP) on some events day (e.g., events 4 and 7 in GQD-A118 and 9 in

200   DHO-A118) occurring in different propagation path, as well as increase occurring in both propagation paths (e.g., events 3 and
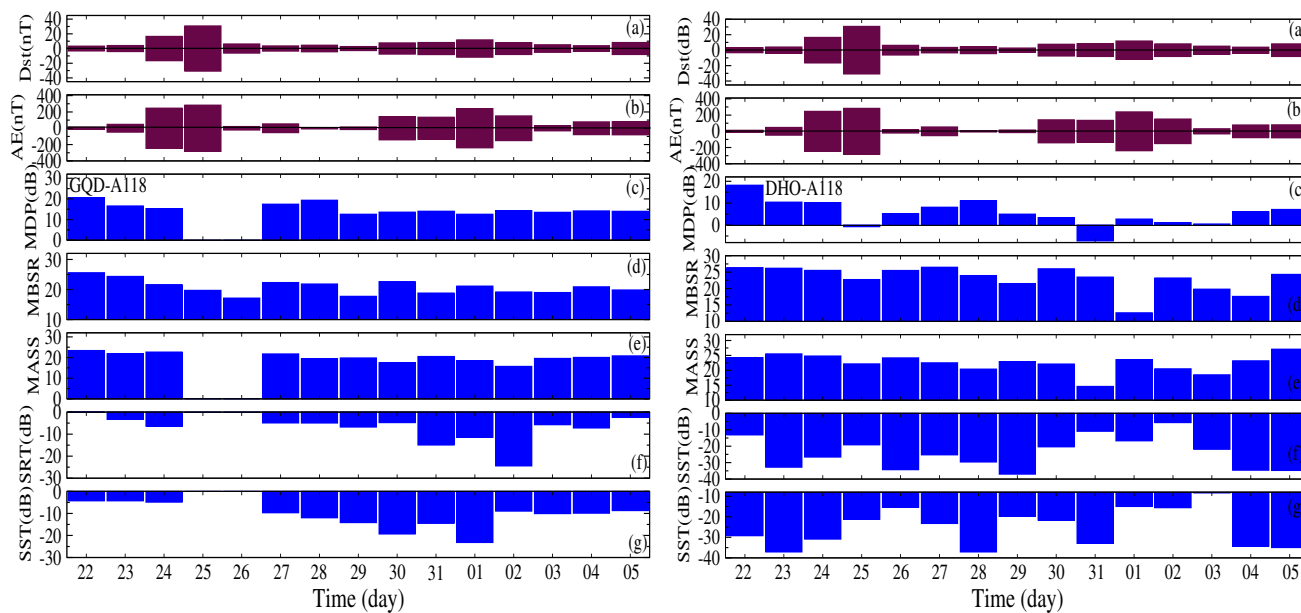
Figure 6. Daily deviations of (a) Dst and (b) AE (c) variations in MDP (d) MBSR (e) MASS (f) SRT and (g) SST for GQD-A118 (left panel) and DHO-A118 (right panel) propagation paths during 22 October - 5 November 2011.

Table 1. Summary of analysed 15 geomagnetic storm events

No.	Date	Max Dst (nT)	σ_{Dst}	Flare count(C M X)
1	26092011	-101	±50.73	9 2 0
2	25102011	-132	±30.76	1 0 0
3	22012012	-67	±37.00	4 0 0
4	15022012	-58	±9.63	0 0 0
5	19022012	-54	±12.8	1 0 0
6	07032012	-74	±25.41	1 0 0
7	15032012	-74	±20.75	1 0 0
8	28032012	-55	±12.09	1 0 0
9	05042012	-54	±13.82	3 0 0
10	23042012	-95	±32.23	3 0 0
11	12062012	-51	±12.47	13 0 0
12	16062012	95	±20.24	4 0 0
13	15072012	-126	±47.88	8 0 0
14	02092012	-54	±13.86	5 0 0
15	09102012	-105	±25.64	10 1 0

12). While the probable reason for the former scenario is suggestive of factors such as propagation characteristics and X-ray flux induced spike in amplitude, further investigation into why this characteristic exist will be pursued. To further check this scenario, we study and show variations in X-ray flux output and geomagnetic indices on the particular day of the events (3 and 12) to better interpret the prevailing ionospheric conditions at the time.

205

Table 2. Summary of trend in dipping of the signals' metrics during 15 geomagnetic storm case in (a) DHO-A118 and GQD-A118 propagation path

Signal (dB)	GQD-A118 propagation path			DHO-A118 propagation path		
	Available data	No. of dips	% dip	Available data	No. of dips	% dip
MDP	12	8	67	15	12	80
MBSR	13	10	77	15	9	60
MASS	12	7	58	15	10	67
SRT	12	3	25	15	5	33
SST	12	5	42	15	7	47

In Figure 8, we show the diurnal VLF amplitude for (a) DHO-A118 and (b) GQD-A118 propagation paths, daily variation in (c) X-ray flux output (d) V_{sw} (e) PD and (f) Dst indices for a day before and after each of the 15 storms condition. Data showed (Fig. 8c, Fig. 8f) the occurrence of M-class flare in association with the storm on 22-23 January 2012 (event 3 on 21 January), both events almost having corresponding peaks during events. This scenario suggest an enhancement of both the
210 instantaneous and background X-ray flux output (as stated earlier), that causes increase (or, spike) in the signal level. Thus probably overshadowed geomagnetic effects on the signal. Whereas this explanation may be argued for events 1 (25-27 Sept. 2011) and 6 (6-8 Mar. 2012), it should be noted that such flare events started well before the storms, and continued until the storms time (in each case), suggesting an established increase in the overall background X-ray before the storms. Hence, a storm induced dipping of the signal from the already existing flux background is speculated on the storm days. However, fur-
215 ther investigation is encouraged, which is beyond the scope of this work. For event 12 (during 15-17 July 2012), we observed that the peak of the storm (that commenced by midnight on 16th) was on 17th (recognised as AEv). Therefore, any geomagnetic influence on the signal (e.g., dipping) is expected on 17th (or, after) and not 16th, hence we observed a dipping of the AEv signal (on 17 Sept.) instead in DHO-A118 propagation path.

220 Figure 9 shows Dst deviation (fluctuation) and 2-day mean variations of MDP, MBSR, MASS, SRT and SST signals before, during and after each event for (a) GQD-A118 and (b) DHO-A118 propagation paths. This analysis is important for corroborating the result presented in Figure 7, because its data selection criterion differ from those of Figure 7 in some ways. While BE, DE and AEv represent data for three consecutive days with reference to the event's day (DE) in the former analysis (presented in Fig. 7), each acronym (BE, DE or AEv) represent a 2-day mean (VLF) with respect to DE (but not necessarily in succession
225 to DE). However, it should be noted that due to the data averaging (2-day), a 'pronounced' increase or dipping in the signals
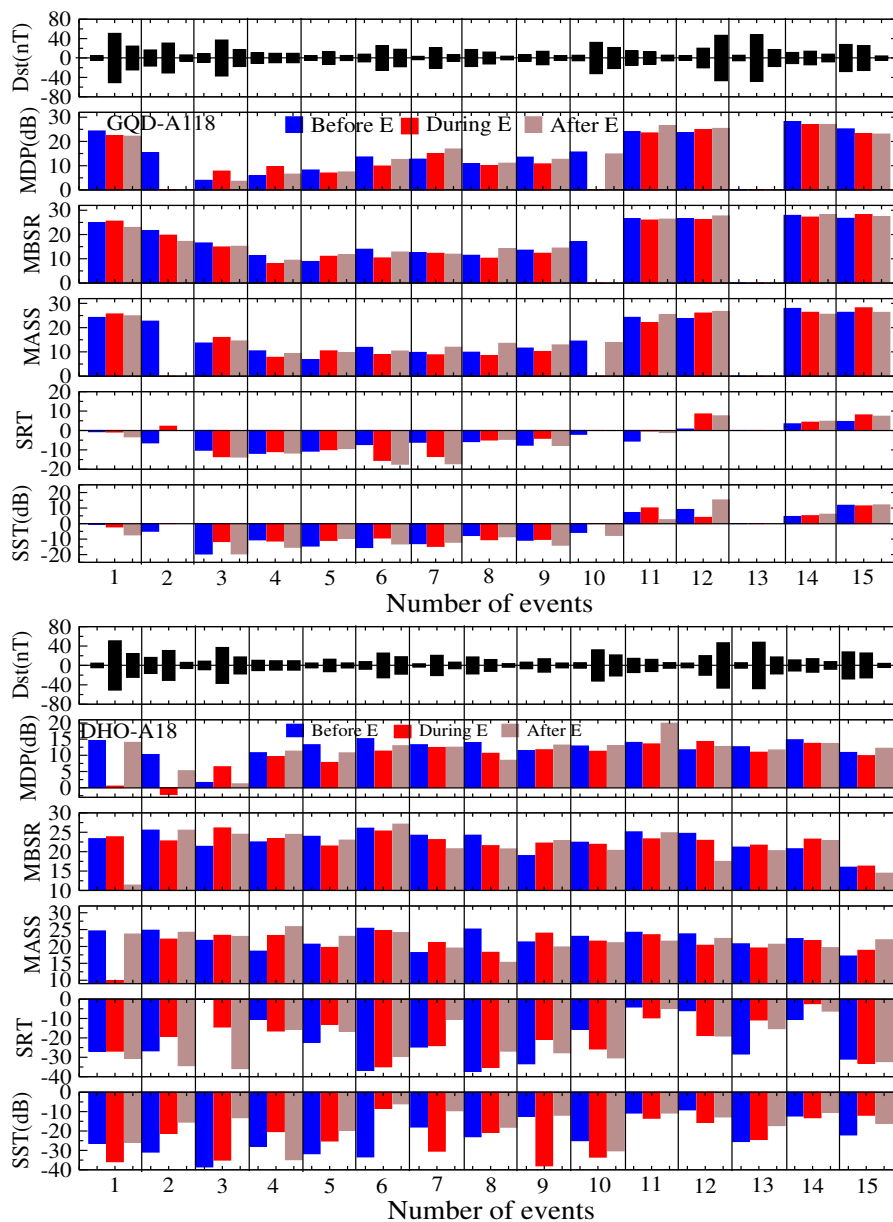
Figure 7. Dst deviation (or fluctuation), and variations in MDP, MBSR, MASS, SRT and SST signals 1-day before, during and after each of the 15 events for GQD-A118 and DHO-A118 propagation paths. Note that the each Dst bar represent the deviation (σ) corresponding to the VLF amplitude before, during and after the events (storm) as listed in Table 1 and shown in figure 8.
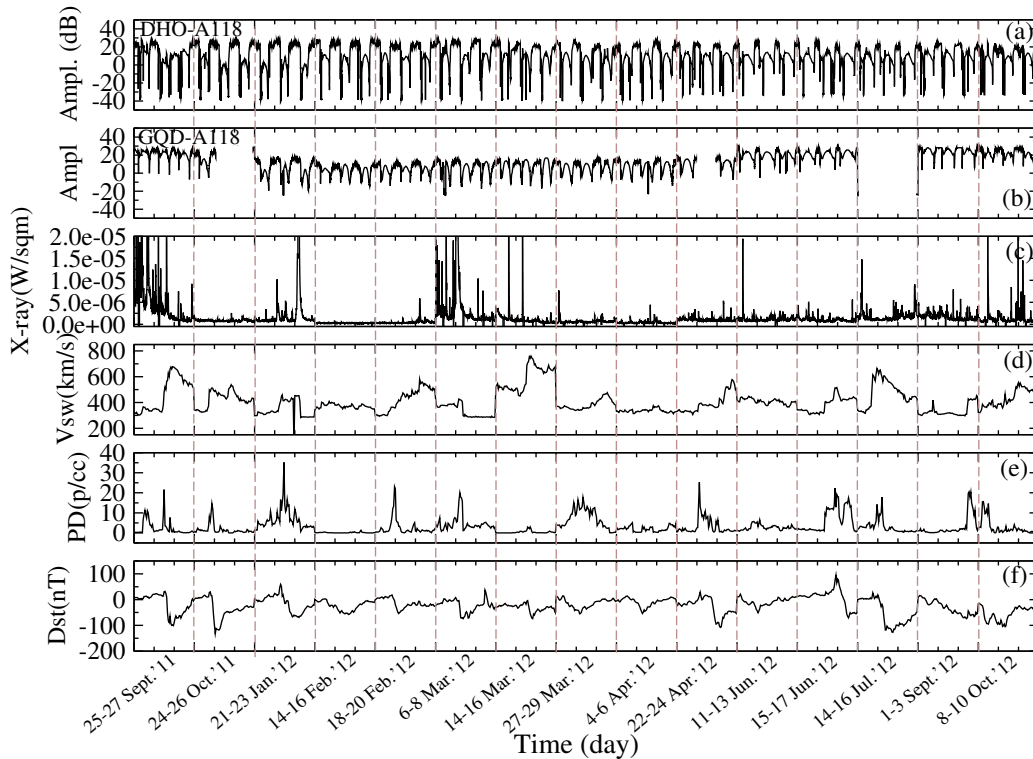
Figure 8. Diurnal VLF amplitude for (a) DHO-A118 and (b) GQD-A118 propagation paths, daily variation in (c) X-ray flux output (d) V_{sw}, (e) PD and (f) Dst indices for a day before and after each of the 15 storms

(comparable to those in the former analysis (fig 7)) are not expected. Another important data selection criterion for this analysis is a relative geomagnetic quiet day BE and AEv with respect to DE.

In GQD-A118 propagation path, 7 of 12 MDP, 7 of 13 MBSR, 7 of 12 MASS, 6 of 12 SRT and 3 of 12 SST showed dipping
230 following the storms, while 10 of 15 MDP, 11 of 15 MBSR, 11 of 15 MASS, 6 of 14 SRT and 6 of 15 SST showed dipping in DHO-A118 propagation path. These values correspond to respective 62.5%, 63.5%, 65.5%, 46.5% and 32.5% of the combined cases. The signal levels, along with the percentage dip of the signals are presented in Table 3. In general, the trend of variation of the signal metrics considerably reflected the prevailing space weather coupled effects in the lower ionosphere. The MDP signal appears to be more responsive (about 68% for combined analysis shown in figs 7 and 9) to geomagnetic perturbations
235 than other signal metrics. However, we anticipate an improvement with analysis of smaller range calculation of mean values of MBSR and MASS due to high fluctuation of dusk-to-dawn D region ionosphere (as was done in Nwankwo et al. (2020d). Also analysis of the DTMA instead of the MDP improved the results (e.g., Nwankwo et al. 2020d). Nwankwo et al. (2016) noted the existence of pseudo-SRT and SST exhibited by diurnal VLF signal (see, Fig. 2c) as drawback in SRT and SST analysis.
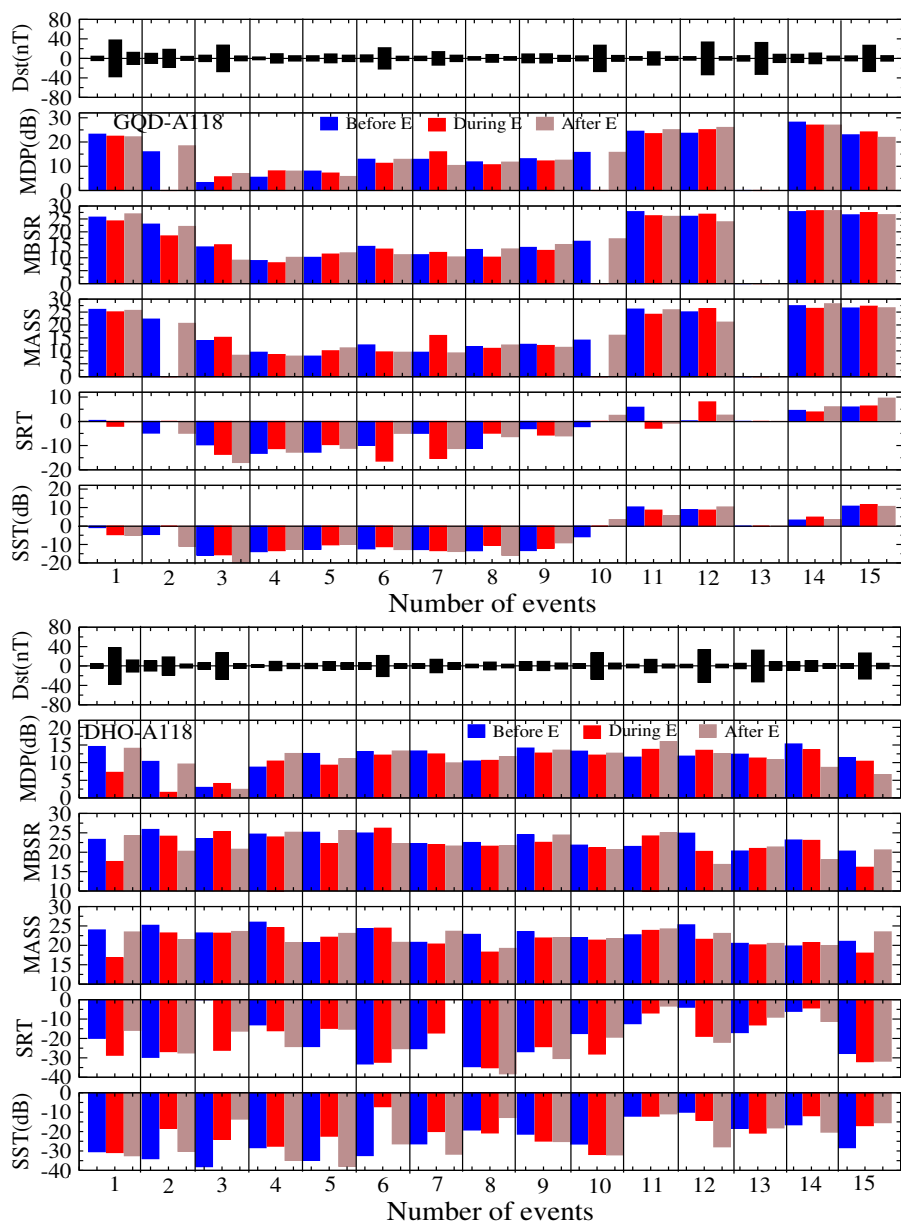
Figure 9. Dst deviation and 2-day mean variations of MDP, MBSR, MASS, SRT and SST signals before, during and after each event for GQD-A118 and DHO-A118 propagation paths.

This anomaly is due to secondary destructive interference pattern in signals and occurrence of solar flares during sunrise/sunset
240 (Chakrabarti, personal com., 2016). Authors concluded in their study that the post-storm SRT and SST variations do not appear
to have a well-defined trend associated with storm effect based on the appraoch utilised (Nwankwo et al., 2016). In this work,
we considered the 'first' SRT and SST values (in the event of a pseudo-terminator) during analysis of the signal metrics. A rise
in SRT and SST amplitude under geomagnetic storm conditions appear to occur more than otherwise in both propagation paths
in this analysis; we found a respective dipping of 46.5% and 32.5% of the SRT and SST in the combined cases. However, this
245 need to be investigated further. It is important to note that out of the two propagation paths used in this study, the DHO-A118
signal appears to be more sensitive to geomagnetic storm-induced magnetosphere-ionospheric dynamics. We do not expect a
'perfect' consistency in signal trend and variations across all cases, because the individual effects of solar and other forcing
mechanisms (including those of lithospheric and atmospheric sources) on the ionosphere are difficult to estimate (Kutiev, 2013;
Nwankwo et al., 2016). This scenario can also cause non-linear coupling processes and consequent significant fluctuations in
250 radio signals.

Table 3. Summary of trend in 2-day mean signals dipping following 15 geomagnetic storm case in (a) DHO-A118 and GQD-A118 propagation path

Signal (dB)	GQD-A118 propagation path			DHO-A118 propagation path		
	Available data	No. of dips	% dip	Available data	No. of dips	% dip
MDP	12	7	58	15	10	67
MBSR	13	7	54	15	11	73
MASS	12	7	58	15	11	73
SRT	12	6	50	14	6	43
SST	12	3	25	15	6	40

3.2 Investigating the state of the ionosphere over the propagation paths of the VLF signals

Here, we study the state of the ionosphere over the two VLF propagation paths using the virtual heights (h'E, h'F1 and h'F2)
and critical frequencies ($f o$E, $f o$F1, and $f o$F2) of the E and F regions obtained from two ionosonde stations near the GQD and
DHO transmitters. Although we aimed at obtaining data from stations near each transmitter/receiver and at the mid-point, we
255 found no ionosonde station at the mid-point, and the nearest station to the receiver (Tortosa) has no data for the period/intervals
under study. However, to make up for this dearth of data, we will complement the analysis with the results in the extended
study that utilised the GNSS data in the region (e.g., (Nwankwo et al., 2020d)). Details of the ionosonde stations used in this
study are provided in Table 4. We treat Chilton station as nearest to GQD transmitter and Juliusruh station nearest to DHO
transmitter. Tortosa station is closest to the A118 transmitter but has no data for the intervals. We obtained and calculated the
260 daytime (8:00 am - 3:00 pm) mean values and standard deviations (σ) of the parameters, and analysed for the storms of interest
(on 17 and 26 September and 1 November) within the intervals 16-19, 25-28 September and 29 October to 2 November 2011.

We exclude analysis of the 25 October storm because the data for this interval are inadequate.

Table 4. Ionosode stations near the VLF transmitters, receiver and/or propagation paths

Station	Location	Coordinate	Nearest Transmitter/Receiver	Approx. dist. from Transmitter/Receiver
Chilton	United Kingdom	51.5696°N, 1.2997°W	GQD	394.15 km
Juliusruh	Germany	54.6207°N, 13.3719°E	DHO	415.71 km
Tortosa	Spain	40.8126°N, 0.5214°E	A118	301.87 km

Figure 10 shows the daily mean and standard deviation (SD or σ) of foF2, foF1, foEs, foE, h'F2, h'F, h'Es and h'E during 16-17 September 2011 for Chilton and Juliusruh Stations. We compare the pre-storm day (blue broken line) values with the storm day (red broken line) values. At Chilton station (near the GQD transmitter) result show significant increase and/or fluctuation (increase in SD) of the foF2, and a decrease (with significant fluctuation) of foF1 on the storm day, 17 September. The height of the E and F regions (h'F2, h'F, h'Es and h'E) significantly increased following the storm. Similar pattern of variations were observed at Juliusruh station. The foF2 and foF1 increased (and/or fluctuated) significantly, as well as h'F2, h'F, h'Es and h'E. Values of foEs decreased, while the foE remained unaffected in both stations. Also, there appear to be a sustained post-storm increase and/or fluctuations of the parameters on on 18 September, suggesting a continuous driving of the ionosphere by the storm.

Figure 11 show the daytime mean variations and SD of foF2, foF1, foEs, foE, h'F2, h'F, h'Es and h'E during 25-28 September 2011 for Chilton and Juliusruh Stations. The storm during this interval (on 26 September) is well developed (with Dst up to -101 nT) and larger than the 17 September event. The result of this analysis show a slight increase of foF2 and foF1 but a decrease in foEs and foE for Chilton station. The height of the F2 (h'F2) decreased (by 6.90 km) while those of the F, Es and E increased on the storm day, 26 September. Near the DHO transmitter (Juliusruh station) there is an anti-correlated variation in the critical frequencies of the E and F regions; a depression of the foF2 and foF1, but increase in foEs and foE (when compared with the scenario at Chilton station). The height of the F2, F and E regions increased by 47.89 km, 16.08 km and 9.14 km, respectively (which are so far the largest increase of the parameters), while the height of the Es region decreased by only 0.16 km (see, Table 5).

Figure 12 show the daytime mean variation and SD of foF2, foF1, foEs, foE, h'F2, h'F, h'Es and h'E during 29 October - 02 November 2011 for Chilton and Juliusruh Stations. This interval is of interest because of the fluctuation in geophysical parameters during the days preceding the storm. The goal of including this interval is to investigate the couple effect of this extended period of (30-31 Oct.) of geomagnetic disturbances preceding the storm on 1 November. It appears that energy began building up in the magnetosphere-ionosphere system after the first significant spike in V_{sw} and PD around 10:00 am on 30
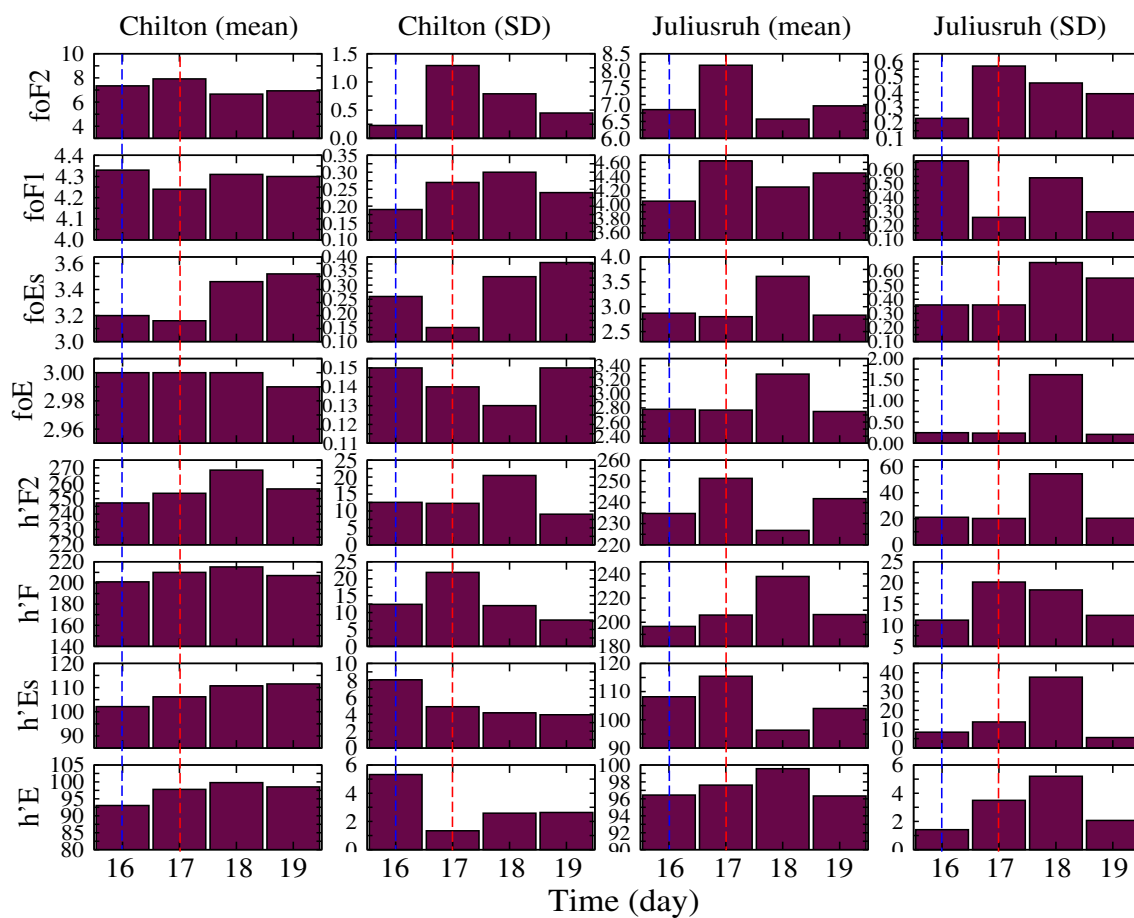
Figure 10. Daytime mean variations and standard deviation (SD) of foF2, foF1, foEs, foE, h'F2, h'F, h'Es and h'E during 16-17 September 2011 for Chilton and Juliusruh Stations. The blue broken line represent the pre-storm day values, while the red broken line represent the storm day values of the ionospheric parameters.
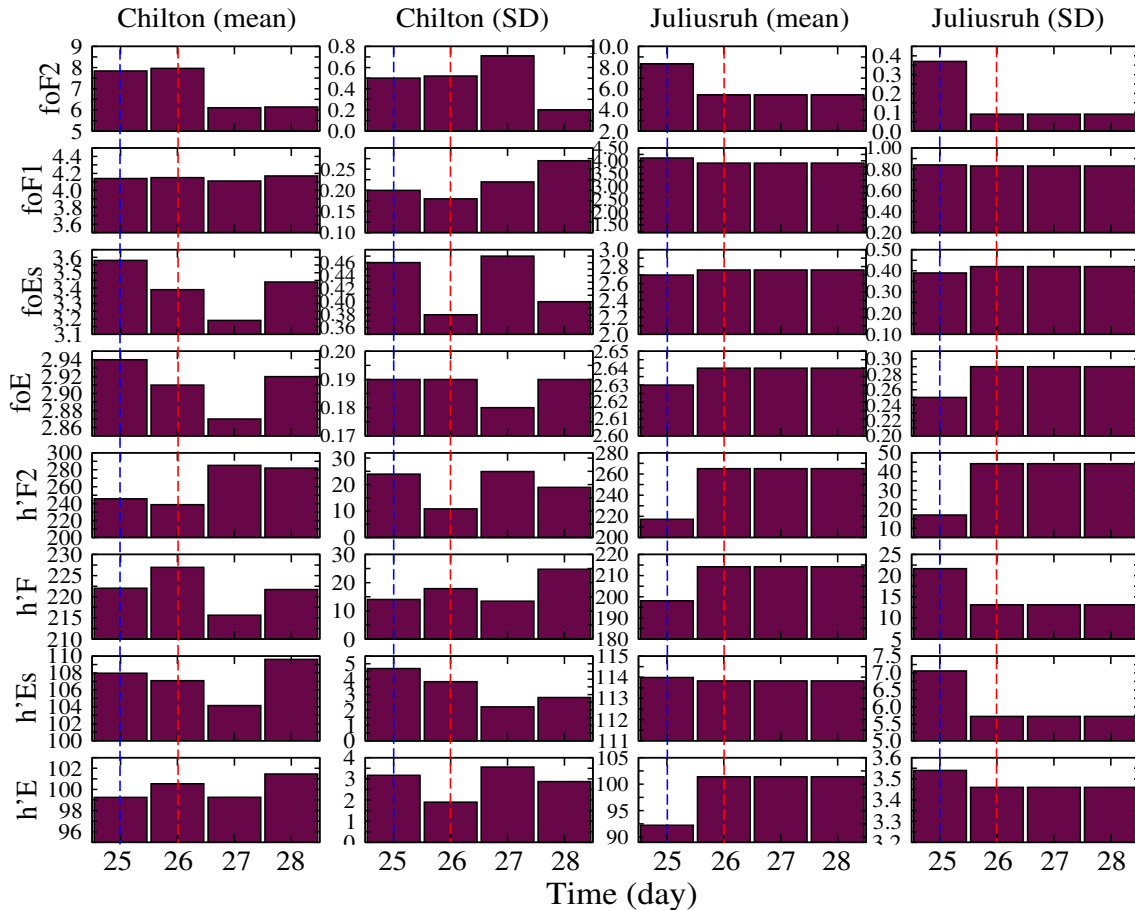
Figure 11. Daytime mean variation and SD of foF2, foF1, foEs, foE, h'F2, h'F, h'Es and h'E during 25-28 September 2011 for Chilton and Juliusruh Stations

October until around 10:00 am on 1 November when the storm was triggered following sudden increased in V_{sw} and south-
290   ward turning of the B_z (Nwankwo et al. 2020d). Here, we compare the parameters' level on the relatively quiet day (29 Oct.)
with those of the storm day (on 1 Nov.), since the two days preceding the storm were signicantly disturbed. The result show
significant increase of foF2 and foF1 at Chilton station. Like the 17 September storm scenario, values of foEs decreased, while
the foE remained unaffected for this station. The h'F2 decreased, while the h'F, h'Es and h'E showed an increased. At Juliusruh
station only the critical frequency of the F2 region increase, while those of the F1, Es and E decreased. However, the increase
295   and/or fluctuation of the parameters were significant (in most cases) during the disturbed days (30 and 31 Oct.) preceding
the storm, suggesting coupled responses of ionosphere before the storm commencement (as a result of increased geomagnetic
activity on the days). We present summary of the storms day variations in h'F2, h'F, h'Es and h'E for the two stations in Table 5.
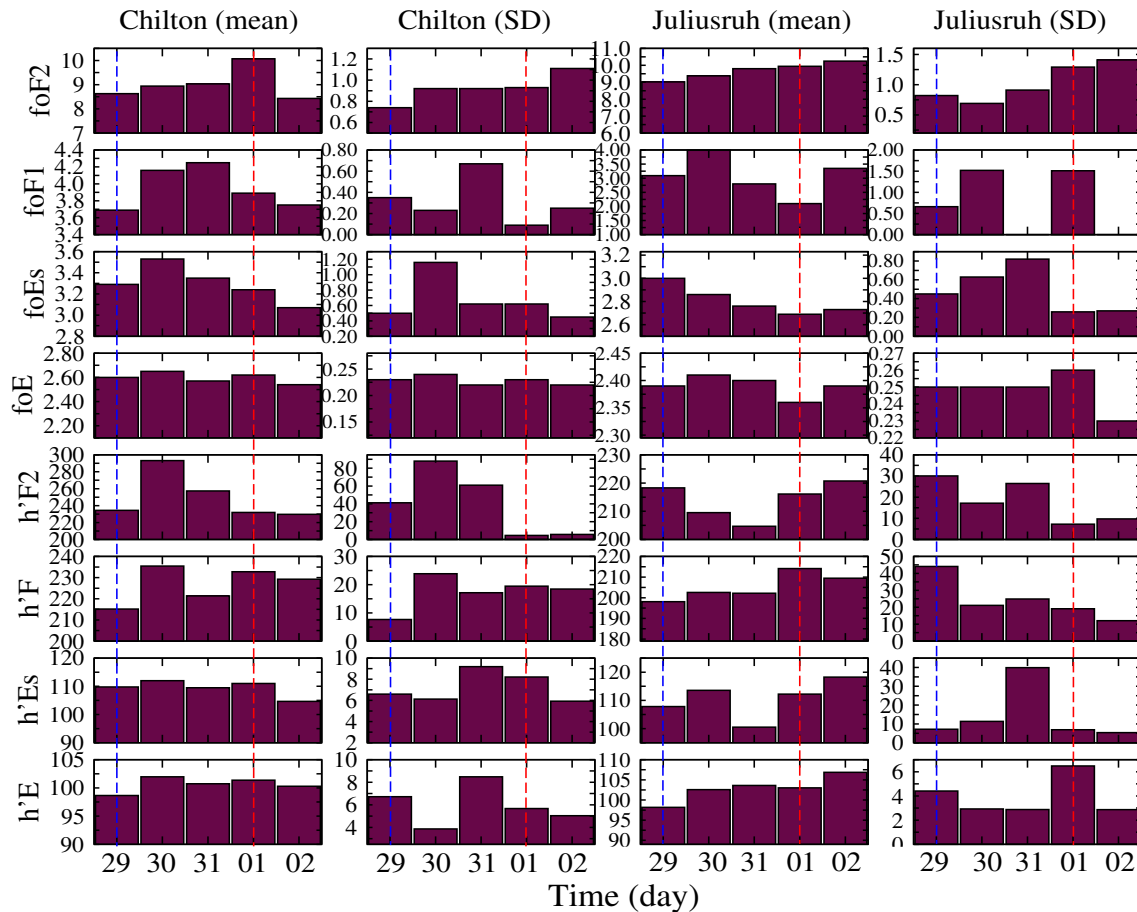
Figure 12. Daytime mean variation and SD of foF2, foF1, foEs, foE, h'F2, h'F, h'Es and h'E during 29 October - 02 November 2011 for Chilton and Juliusruh Stations.

In summary, foF2, foF1, h'F2, h'F, h'Es and h'E generally showed significant increase and/or fluctuation near both trans-
300 mitters (GQD and DHO) during the geomagnetic storms, whereas foEs and foE either increased (slightly) or unaffected. It appears that the observed storm-induced increase and fluctuation are largely sustained or further enhanced on the day (or days) following the event (post storm day), suggesting a continuous driving of the ionosphere by the storms. Although the analysis for 1 November storm scenario showed weak correlation, variations of the parameters reflected the coupled responses of the ionosphere to energy build-up ahead of storm commencement. Nwankwo and Chakrabarti (2018) reported significant
305 depression and fluctuations of foF2 following significant geomagnetic disturbances and/or storms in high- and mid-latitude, and distortion in the quasi-periodic pattern of the parameter. Their inference was, however, based on a preliminary analysis from the result of single ionosode station. From this comparatively detailed analysis, it is clear that the reported depression of foF2 may occur during some (isolated) storms and locations, and should, therefore, not be treated as global response. Negative

storm effects (in which foF2 assumes a negative values) has also been reported (e.g., (Blanch et al., 2013; Kane, 2005)). In

310 this analysis, the largest increase of the h'F2, h'F, h'Es and h'E occured in Juluisruh, near the DHO transmitter (see Table 5). This observation is instructive! When justaposed with the analysis of VLF signals variation during the storms (section 2.2) we connect the observed larger ionosode increase or responses with the larger amplitude decreases in the DHO-A118 propagation path signal, and infer that the effect of the storms appear to be more intense (strong responses) around or near the DHO receiver or DHO-A118propagation path. This result is in agreement with the recent findings reported in Nwankwo et

315 al. (2020d). Their study combined observed VLF amplitude variations with TEC/VTEC data obtained from multiple GNSS stations (including Euskirchen (Germany), Hailsham (UK), Paris (France) and Naut Aran (Spain)), to investigate ionospheric response to storms over some signal propagation paths during the same events. They showed simultaneous increase of VLF amplitude and enhancement of electron density profiles near the DHO transmitter.

Table 5. Observed increase (or decrease) of the foF2, foF, foEs and E during the storms on 17 and 25 September and 1 November 2011

	17 Sept. storm		26 Sept. storm		1 Nov. storm	
Parameter	Chilton	Juliusruh	Chilton	Juluisruh	Chilton	Juluisruh
h'F2	6.46 km	16.57 km	-6.90 km	47.89 km	-2.00 km	-2.18 km
h'F	8.92 km	9.42 km	4.92 km	16.08 km	17.65 km	16.04 km
h'Es	4.04 km	7.25 km	-0.88 km	-0.16 km	1.25 km	4.41 km
h'E	4.78 km	1.18 km	1.29 km	9.14 km	2.71 km	4.82 km

4 Conclusions

320 In this work, we performed a diagnostic study of geomagnetic storm-induced disturbances that are coupled to the lower ionosphere in mid-latitude D-region using propagation characteristics of VLF radio signals. We characterised the diurnal signal into five metrics (i.e MBSR, MDP, MASS, SRT and SST), and monitored the trend in variations of the signal metrics for up to 20 storms between September 2011 and October 2012. The goal of the analysis is to understand deviations in the signal that are attributable to the storms. Up to five (5) storms and their effects on the signals were studied in detail, followed by statistical

325 analysis of 15 other cases. Our results showed that the MDP exhibited characteristic dipping in about 67% and 80% of the cases for GQD-A118 and DHO-A118 propagation paths, respectively. The MBSR showed respective dipping of about 77% and 60%, while the MASS dipped by 58% and 67%. Conversely, the SRT and SST showed respective dipping of 25% and 33%, and 42% and 47%, favouring rise of the signals following storms. Of the two propagation paths used in this study, the dipping of the amplitude of DHO-A118 propagation path during the storms is larger. To understand the state of the ionosphere over the

330 propagation paths and how it affects the VLF responses, we further analysed virtual heights ($h'E$, $h'F1$ and $h'F2$) and critical frequencies (foE, $foF1$, and $foF2$) of the E and F regions (from ionosonde stations near the GQD and DHO transmitters). The results of this analysis showed a significant increase and/or fluctuation of the foF2, foF1, h'F2, h'F, h'Es and h'E near both transmitters during the geomagnetic storms. We found that the largest increase in the height of the regions (h'F2, h'F, h'Es and

h'E) occured in Juluisruh (Germany), near the DHO transmitter, suggesting a strong storm responses over the region possibly
335   leading to the large dipping of VLF amplitude for DHO-A118 propagation path.

Competing interests. The authors declare that they have no conflict of interest

Acknowledgements. V.U.J. Nwankwo acknowledge the World Academy of Science (TWAS), Trieste, Italy and the S.N. Bose National
Centre for Basics Sciences (SNBNCBS) for the awarde of Postgraduate research fellowship during which a portion of this work was done.
The authors thank Dr. Bruce Tsurutani (Jet Propulsion Laboratory, California Institute of Technology) and Dr. Jan Lastovicka for clarification
340   of some aspects of geomagnetic data and processes. We also acknowledge the UK Solar System Data Centre (UKSSDC) for ionosonde data.

References

Alfonsi L., Andrew J. Kavanagh, Ermanno Amata et al. (2008), Probing the high latitude ionosphere from ground-based observations: The state of current knowledge and capabilities during IPY (2007-2009), J Atm. Solar-Terres. Phys., 70, 2293 - 2308.

Araki T. (1974), Anomalous Phase Changes of Trans equatorial VLF Radio Waves during Geomagnetic Storms, J Geophys. Res., 79, 4811-4813

Baker D. N. (2000), Effects of the Sun on the Earth's environment, J. Atm. Solar-Terres. Phys., 62, 1669-1681.

Blanch, E., S. Marsal, A. Segarra, J.M. Torta, D. Altadill, and J.J. Curto (2013), Space weather effects on Earth's environment associated to the 24-25 October 2011 geomagnetic storm, Space Weather, 11, 153-168, doi:10.1002/swe.20035.

Borovsky J. E. and Denton M. H. (2006), Differences between CME-driven storms and CIR-driven storms, J Geophys. Res., 111

Bucha V. and Bucha Jr. V., Geomagnetic forcing of changes in climate and in the atmospheric circulation, J. Atmos. Sol-Terr. Phys., 60, 145 - 169.

Buonsanto M.J. (1999), Ionospheric storms: a review, Space Sci. Rev., 88, 563 - 601.

Buresova D. and Lastovicka J. (2007), Pre-storm enhancements of foF2 above Europe, Adv. Space Res. 39, 1298-1303.

Burke W. J. (2000), Magnetosphere-ionosphere coupling: selected topics, J Atmo. Solar-Terres. Phys., 62, 817-824.

Burns A. G., S.C. Solomon, L. Qian, W. Wang, B.A. Emery, M. Wiltberger, and D.R. Weimer (2012), The effects of Corotating interaction region/High speed stream storms on the thermosphere and ionosphere during the last solar minimum, J Atm. Solar-Terres Phys., 83, 79-87

Chenette D.L., Datlowe D. W., Robinson R. M., Schumaker T. L., Vondrak R. R., and Winningham J. D. (1993), Atmospheric energy input and ionization by energetic electrons during the geomagnetic storm of 8-9 November 1991, Geophys. Res. Lett., 20, 1323.

Clilverd M. A., Rodger C. J., Gamble R. J., Ulich T., Raita T., Seppala A., Green J. C., Thomson N. R., Sauvaud J. A., and Parrot M. (2010), Ground-based estimates of outer radiation belt energetic electron precipitation fluxes into the atmosphere, J Geophys. Res., 115, A12304.

Cowley S. W. H., Davies J. A., Grocott A., Khan H., Lester M., McWilliams K. A., Milan S. E., Provan B., Sandholt P. E., Wild J. A. and Yeoman T. K. (2003), Solar-wind-magnetosphere-ionosphere interactions in the Earth's plasma environment, Phil. Trans. R. Soc. Lond. A, 361, 113-126.

Chuo, Y. J., C. C. Lee, W. S. Chen, and B. W. Reinisch (2013), Comparison of the characteristics of ionospheric parameters obtained from FORMOSAT-3 and digisonde over Ascension Island, Ann. Geophys., 31, 787-794.

Danilov A. D. and Lastovicka J. (2001), Effects of Geomagnetic Storms on the Ionosphere and Atmosphere, Inter. J. Geomagn. Aeron., 2, 209-224.

Gosling J.T. and Pizzo V.J. (1999), Formation and evolution of corotating interaction regions and their three dimensional structure, Space Sci. Rev. 89, 2152.

Heikkila W. (2011), Earth's Magnetosphere, Elsevier Kidlington, Oxford, UK.

Kane R.P. (2005), Ionospheric f oF2 anomalies during some intense geomagnetic storms, Ann Geophys., 23, 2487-2499.

Kelley M. C. (1989), The Earth's Ionosphere, Academic Press Inc. San Diego, California.

Kikuchi T. and Evans D.S. (1983), Quantitative study of substorm-associated VLF phase anomalies and precipitating energetic electrons on November 13, 1979, J. Geophys. Res., 88, 871-880.

Kleimenova N. G., Kozyreva O. V., Rozhnoy A. A. and Soloveva M. S. (2004), Variations in the VLF signal parameters on the Australia-Kamchatka radio path during magnetic storms, Geomagn. Aeron. 44, 385-393.

Koga D., Sobral J. H. A., Gonzalez W. D., Arruda D. C. S., Abdu M. A., deCastilho V. M., Mascarenhas M., Gonzalez A. C., Tsurutani B. T., Denardini C. M., and Zamlutti C. J. (2011), Electro-dynamic coupling processes between the magnetosphere and the equatorial ionosphere during a 5-day HILDCAA event, J. Atmos. Solar Terr. Phys., 73, 148-155.

380 Kozyra J. U, G. Crowley, B. A. Emery, X. Fang, G. Maris, M. G. Mlynczak, R. J. Niciejewski, S. E. Palo, L. J. Paxton, C. E. Randall, P.P. Rong, J. M. Russell III, W. Skinner, S. C. Solomon, E. R. Talaat, Q. Wu and J.H. Yee (2006), Response of the Upper/Middle Atmosphere to Coronal Holes and Powerful High-Speed Solar Wind Streams in 2003. Recurrent Magnetic Storms: Corotating Solar Wind Streams. Geophysical Monograph 167. Edited by Bruce Tsurutani, Robert McPherron, Walter Gonzalez, Gang Lu, Jose H. A. Sobral and Natchimuthukonar Gopalswamy. ISBN-13: 978-0-87590-432-0. AGU Books Board, AGU, Washington, DC USA, 319.

385 Kumar A. and Kumar S. (2014), Space weather effects on the low latitude D-region ionosphere during solar minimum. Earth, Planets and Space, 66.

Kutiev I., Ioanna Tsagouri, Loredana Perrone, Dora Pancheva, Plamen Mukhtarov, Andrei Mikhailov, Jan Lastovicka, Norbert Jakowski, Dalia Buresova, Estefania Blanch, Borislav Andonov, David Altadill, Sergio Magdaleno, Mario Parisi and Joan Miquel Torta (2013), Solar activity impact on the Earth's upper atmosphere, Journal of Space Weather and Space Climate, 3.

390 Lastovicka J. (1989), Solar wind and high energy particle effects in the middle atmosphere, Handb. MAP, 29, 119.

Lastovicka J. (1996), Effects of geomagnetic storms in the lower ionosphere, middle atmosphere and troposphere, J. Atm. Sol. Terr. Phys., 58, 831-843.

Lu G., Cowley S. W. H., Milan S. E., Sibeck D. G., Greenwald R. A., Moretto T. (2002), Solar wind effects on ionospheric convection: a review, J. Atm. Solar-Terr. Phys., 64, 145-157.

395 McPherron R., Weygand J., Tung-Shin Hsu (2008), Response of the Earth's magnetosphere to changes in the solar wind. J. Atm. Solar-Terr. Phys., 70(2), 303-315. DOI: 10.1016/j.jastp.2007.08.040

McRae W. M. and Thomson N. R. (2004), Solar flare induced ionospheric D-region enhancements from VLF phase and amplitude observations, J Atm. Solar-Terres. Phys., 66, 77-87. DOI:10.1016/j.jastp.2003.09.009

Mitra W. B. (1974), Ionospheric effects of solar flares, D. Reidel Publishing Company, Dordrecht, Holland.

400 National Geographic Data Centre, 1996. Ionospheric Digital Database: Worldwide Vertical Incidence Parameters. National Geographic Data Centre, NOAA Boulder, Colorado, USA.

NOAA SWPC (Retrieved 2012), Solar Particle and Geomagnetic Indices. $swpc.noaa.gov/ftpmenu/indices/old\_indices.html$

NOAA SWPC (Retreived 2015), Solar wind speed, proton/particle density and magnetic field components. $ftp://sohoftp.nascom.nasa.gov/sdb/goes/ace/$

405 NOAA SWPC (Retrieved 2015), Auroral Electrojet (AE) Index. $ftp://ftp.ngdc.noaa.gov/STP/GEOMAGNETIC_DATA/INDICES/AURORAL_ELECTROJET/$

NOAA (Retrieved 2016), Geomagnetic Storms, NOAA Space Weather Prediction Center, $http://www.ngdc.noaa.gov/phenomena/geomagnetic-storms$

Nwankwo V. U. J., Chakrabarti S. K. and R. S. Weigel (2015), Effects of plasma drag on low Earth orbiting satellites due to solar forcing induced perturbations and heating, Adv. Space Res., 56, 47-56.

410 Nwankwo V. U. J., Chakrabarti S. K. and Ogunmodimu O. (2016), Probing geomagnetic storm-driven magnetosphere-ionosphere dynamics in D-region via propagation characteristics of very low frequency radio signals, J. Atmos. Sol-Terres. Phys., 145, 154-169.

Nwankwo, V.U.J. and Chakrabarti, S.K. (2018) Effects of space weather on the ionosphere and LEO satellites' orbital trajectory in equatorial, low and middle latitude. Adv. Space Res., 61(7), 1880-1889, doi:https://doi.org/10.1016/j.asr.2017.12.034.

Nwankwo V.U.J., Chakrabarti S.K., Sasmal S., Denig W. et al. (2020b). Radio aeronomy in Nigeria: First results from very low frequency
415   (VLF) radio waves receiving station at Anchor University, Lagos. 2020 IEEE-ICMCECS, Lagos, Nigeria, pp 1-7, DOI: 10.1109/ICM-
        CECS47690.2020.247002.

Nwankwo V.U.J., Raulin J-P., Correia E., Denig W., Folarin O. and Ogunmodimu O. (2020d), Investigation of ionosphere response to
        geomagnetic storms over the propagation paths of very low frequency radio waves. [Submitted]

Ouattara, F., Amory-Mazaudier, C., Fleury, R., Lassudrie Duchesne, P., Vila, P.,Petitdidier, M. (2009), West African equatorial ionospheric
420   parameters climatology based on Ouagadougou ionosonde station data from June 1966 to February 1998. Ann. Geophys. 27, 2503-2514.

Peter W. B., Chevalier M. W., and Inan U. S. (2006), Perturbations of mid-latitude sub-ionospheric VLF signals associated with lower
        ionospheric disturbances during major geomagnetic storms, J Geophys. Res., 111, AO3301.

Prolss G. W. (2004), Physics of the Earth's space environment, Springer Berlin Heidelberg, Germany.

Raulin, J.-P., Pacini, A.A., Kaufmann, P., Correia, E., Martinez, M.A.G. (2010). On the detectability of solar X-ray flares using very low
425   frequency sudden phase anomalies, J Atmo. Solar-Terres. Phys., 68, 1029-1035.

Sica R. J., and R. W. Schunk (1990), Interpreting vertical plasma drift in the mid-latitude ionosphere using ionosonde measurements, J.
        Atmos. Terr. Phys., 38, 1567-1571.

Simoes F., Pfaff R., Berthelier J. and Klenzing (2012), A Review of Low Frequency Electromagnetic Wave Phenomena Related to
        Tropospheric-Ionospheric Coupling Mechanisms, Space Sci. Rev., 168, 551-593.

430 Stoke P. H. (1993), Energetic Electron Power Flux Deposition at Sanae (L=4.0) from Riometer Recording, J Geophys. Res., 98, 19111-19116.

Tatsuta K., Hobara Y., Pal S. and Balikhin M. (2015), Sub-ionospheric VLF signal anomaly due to geomagnetic storms: a statistical study,
        Ann. Geophys., 33, 1457-1467.

Tsurutani B. T., Gonzalez W. D., Gonzalez A. L. C., Tang F., Arballo J. K., and Okada M. (1995), Interplanetary origin of geomagnetic
        activity in the declining phase of the solar cycle, J. Geophys. Res., 100, 21717-21733.

435 Tsurutani B. T., Gonzalez W. D., Gonzalez A. L. C., Guarnieri F. L., Gopalswamy N., Grande M., Kamide Y., Kasahara Y., Lu G., Mann I.,
        McPherron R. L., Soraas F., and Vasyliunas V. M. (2006), Corotating solar wind streams and recurrent geomagnetic activity: A review. J.
        Geophys. Res., 111, A07S01, doi:10.1029/2005JA011273.

Tsurutani B. T., Echer E., Guarnieri F. L. and Gonzalez W. D. (2011), The properties of two solar wind high speed streams and related
        geomagnetic activity during the declining phase of solar cycle 23, J. Atmos. Solar-Terr. Phys., 73, 164, doi:10.1016/j.jastp.2010.04.003.

440 Verkhoglyadova O. P., Tsurutani B. T., Mannucci A. J., Mlynczak M. G., Hunt L. A., and Runge T. (2013), Variability of ionospheric TEC dur-
        ing solar and geomagnetic minima (2008 and 2009): external high speed stream drivers, Ann. Geophys., 31, 263-276, doi:10.5194/angeo-
        31-263-2013.

Wait J. R. (1959), Diurnal change of ionospheric heights deduced from phase velocity measurements at VLF, Proc. IRE, 47, 998.

Wait J. R. and Spies K. P. (1964), Characteristics of the Earth-ionosphere wave-guide for VLF radio waves, NBS Tech. Note 300

445 WDCG (Retrieved 2014), Geomagnetic Equatorial Dst index, World Data Centre for Geomagnetism, $http://wdc.kugi.kyoto-u.ac.jp/dstdir/index.html$

Wei Y., Hong M., Wan W., Du A., Lei J., Zhao B., Wang W., Ren Z., and Yue X. (2008), Unusually long lasting multiple penetration of inter-
        planetary electric field to equatorial ionosphere under oscillating IMF Bz, Geophys. Res. Lett., 35, L02102, doi:10.1029/2007GL032305.

Weigel R. S. (2010), Solar wind density influence on geomagnetic storm intensity, J. Geophys. Res., 115, A09201,
450   doi:10.1029/2009JA015062.

Weigel R. S., Baker D. N., Rigler E. J., and Vassiliadis D. (2004), Predictability of large geomagnetic disturbances based on solar wind conditions, IEEE Trans. Plas. Sci., 32, 1506-1510.